Time-dependent susceptibility of a helium atom in intense laser pulses

A. Spott, A. Jaron-Becker, and A. Becker

Phys. Rev. A **96**, 053404 — Published 9 November 2017

DOI: 10.1103/PhysRevA.96.053404

Time-dependent susceptibility of helium atom in intense laser pulses

A. Spott, A. Jaron-Becker, and A. Becker
JILA and Department of Physics, University of Colorado, Boulder, CO-80309, USA

We analyze the time-dependent nonlinear response of helium atom to a strong laser pulse in form of the induced nonlinear electric susceptibility. Our theoretical predictions are based on ab-initio solutions of the time-dependent Schrödinger equation obtained using a numerical basis state method and the short-time Fourier transform. The results qualitatively reproduce features seen in recent experimental data. In particular, we observe deviations from the adiabatic (field-following) response in the electric susceptibility at high intensities. According to our analysis a shift of the peak towards the front of the pulse and changes in the concavity of the slope in the trailing edge of the pulse can be related to the population of continuum states and bound excited states with high angular quantum number during the interaction of the atom with the laser pulse.

PACS numbers: 42.65.An, 32.80.Wr

I. INTRODUCTION

The intensity dependent refractive index is an important parameter characterizing the nonlinear response of media in the interaction with short intense laser pulses. It plays an important role in strong-field phenomena such as self-focusing and self-phase modulation [1], high harmonic and attosecond pulse generation [2–4] or femtosecond pulse propagation [5–7]. Measurement and theoretical analysis of the nonlinear refractive index in gases and other media have recently gained much interest (e.g., [8–16]) in view of a discrepancy between experimental results concerning the higher order terms in a power series expansion of the refractive index [17–20].

The controversial debate is related to the interpretation of a change from a positive to a negative nonlinear refractive index as a function of laser intensity and the impact of excitation and ionization of the target on this behavior. The change is a crucial factor for an understanding of the mechanisms leading to long-range propagation of intense laser pulses in gases and the atmosphere. Moreover, it occurs at intensities at which there is a transition from a perturbative to a nonperturbative interaction between the electrons and the external laser field [14, 16], which typically is accompanied by the onset of other strong-field phenomena such as above-threshold ionization [21, 22] and high-harmonic generation [23, 24].

Beyond the determination of the intensity dependence [17, 20], recently the variation of the nonlinear refractive index over the course of the interaction of atoms with the laser pulse has been measured [18–20, 25]. At low intensities it was found that the index adiabatically follows the change of the electric field amplitude, while at higher intensities a shift of the position of the peak and changes in the slope have been observed. This was attributed to the generation of plasma by ionization of the medium during the pulse [18]. Therefore, these measurements provide insights into the dynamics of self-phase modulation and self-focusing, relevant for the understanding of femtosecond pulse propagation. Furthermore, the results give a test for the theoretical models used for the calculation of the nonlinear refractive index.

In this article we apply ab-initio solutions of the time-dependent Schrödinger equation, obtained using a numerical basis state method [26], to determine the nonlinear electric susceptibility induced by the interaction of an atom with an intense laser pulse as a function of time. The theoretical predictions confirm the features observed in the experiment and provide information about the influence of the time-dependent population of bound excited states and ionization as well as the coupling between bound and continuum states on the observed temporal variation of the index. Calculations are performed for helium atom, the general conclusions however do not depend on the characteristics of the ground state of the target and are expected to hold for other rare gas atoms as well.

In the next section we outline the methods used for the calculation of the time-dependent nonlinear susceptibility. Next, we present the results for helium atom interacting with laser pulses at a wavelength of 800 nm over a range of peak intensities. Characteristic features, such as a shift of the peak towards the front of the pulse and changes in the concavity of the slope at the trailing edge, are then analyzed in view of the contributions from different parts of the field-free spectrum. We end with a brief summary.

II. THEORETICAL METHOD

We obtain the time-dependent susceptibility $\chi(\omega,\tau)$ from the time dependent dipole moment $\mu(t)$ of an atom interacting with an external field $E(t)$, linearly polarized in z-direction, at frequency ω by applying the short time Fourier transform as:

$$\tilde{\chi}(\omega,\tau) = \frac{\mathcal{F}\left\{\mu(t)w(t-\tau)\right\}(\omega)}{\mathcal{F}\left\{E(t)w(t-\tau)\right\}(\omega)}\,. \tag{1}$$

We note that $\tilde{\chi}$ is a complex quantity. Below we analyze the real part $\chi = \Re(\tilde{\chi})$, which corresponds to the experimentally accessible electric susceptibility. The imaginary part of $\tilde{\chi}$ relates to absorption, which we do not

further consider in the present work. $w(t)$ is a windowing function and τ corresponds to the center of $w(t)$. As windowing function we have chosen in our calculations the Dolph-Chebyshev window [27]. Optimized for the narrowest central bandwidth at a given constant attenuation in the sidelobes, the Dolph-Chebyshev window is usually defined via its discrete Fourier transform [28]:

$$W(k) = \frac{\cos\left(N\cos^{-1}[\beta\cos\left(\frac{\pi k}{N}\right)]\right)}{\cosh\left[N\cosh^{-1}(\beta)\right]} \tag{2}$$

with

$$\beta = \cosh\left[\frac{1}{N}\cosh^{-1}\left(10^{\alpha}\right)\right] , \tag{3}$$

where $k = 1, 2, \ldots, N-1$ is the frequency bin, and N is the total number of frequency bins in the window. The attenuation of the sidelobes is controlled via the parameter α; in our calculations we have used $\alpha = 4$ which sets the attenuation to 80 dB. Test calculations have shown that the results presented below are rather insensitive to variations of α.

We find the time dependent dipole moment as the expectation value of the dipole operator as (we use Hartree atomic units $e = m = \hbar = 1$):

$$\mu(t) = - < \Psi(t)|\hat{\mu}|\Psi(t) > . \tag{4}$$

where $\Psi(t)$ is the solution of the time-dependent Schrödinger equation

$$\left(\frac{\hat{\mathbf{p}}}{2} + V_{SAE}(r) + E(t)\hat{\mu}\right)|\Psi(\mathbf{r},t)\rangle = i\frac{\partial}{\partial t}|\Psi(\mathbf{r},t)\rangle \tag{5}$$

with

$$|\Psi(\mathbf{r},t)\rangle = \sum_{nlm} c_{nlm}(t)|\psi_{nlm}(\mathbf{r})\rangle \tag{6}$$

$$= \sum_{nlm} c_{nlm}(t)|R_{nlm}(r)Y_{lm}(\Omega)\rangle \tag{7}$$

and $R_{nl}(r)$ and $Y_{lm}(\Omega)$ are the radial wave functions and spherical harmonics, respectively, corresponding to the field-free Hamiltonian

$$H_0 = \frac{\hat{\mathbf{p}}}{2} + V_{SAE}(r) \tag{8}$$

with a spherical symmetric single-active-electron potential $V_{SAE}(r)$ of the atom. In the present study we have performed calculations for helium atom using the single active electron potential [29]:

$$V_{SAE}(r) = -\frac{1}{r} - \frac{a_1 e^{-c_1 r}}{r} - \frac{a_2 e^{-c_2 r}}{r} - \frac{a_3 e^{-c_3 r}}{r} \tag{9}$$

with $a_1 = 1.231$, $a_2 = -1.325$, $a_3 = -0.231$, $c_1 = 0.662$, $c_2 = 1.236$, and $c_3 = 0.480$. For a linearly polarized field the basis set can be restricted due to the dipole selection rule ($\Delta m = 0$). We consider the ground state of the helium atom as the initial state and therefore include states with $m = 0$ in the basis set only. In this basis set the dipole operator is defined as:

$$\hat{\mu} = -\sum_{nln'l'} |\psi_{nl0}><\psi_{nl0}|z|\psi_{n'l'0}><\psi_{n'l'0}|, \tag{10}$$

We find the radial functions $u_{nl}(r) = rR_{nl}(r)$ as numerical solutions of the corresponding eigenvalue equation using the Numerov method on a logarithmic one-dimensional finite-space grid with the boundary conditions $u_{nl}(r=0) = u_{nl}(R_0) = 0$ [14, 26]. Due to the finite box size R_0 both bound and continuum parts of the spectrum are discrete. For the present set of calculations we have set $R_0 = 1000$ a.u., and basis states up to $n = 2000$ (corresponding to an energy of about 19 a.u., or about 515 eV) and $l = 70$.

Using the expansion of the full wave function into a set of field-free basis states makes any observables accessible for separation in contributions arising from the different parts of the spectrum of the field-free Hamiltonian. For the dipole moment and the related electric susceptibility we split:

$$\begin{aligned} < \Psi(t)|\hat{z}|\psi(t) > \; = \; & \overbrace{< \Psi(t)|P_{\rm b}^{\dagger}\hat{z}P_{\rm b}|\Psi(t) >}^{\text{bound-bound}} \\ & + \overbrace{< \Psi(t)|P_{\rm c}^{\dagger}\hat{z}P_{\rm c}|\Psi(t) >}^{\text{continuum-continuum}} \\ & + \overbrace{\left[< \Psi(t)|P_{\rm b}^{\dagger}\hat{z}P_{\rm c}|\Psi(t) > + \text{c.c.}\right]}^{\text{bound-continuum}} \end{aligned} \tag{11}$$

where $P_{\rm b}$ is the projection operator onto the field-free bound states which sets $c_{n,l,0} = 0$ for $E > 0$, and $P_{\rm c}$ is the projection operator onto the rest of the spectrum, i.e. the field-free continuum states. Although the separation is done in terms of the field-free states and the characterization of 'bound' and 'continuum' states becomes less applicable during the interaction, it will give us insight concerning the population of states with low and high energy.

III. RESULTS AND DISCUSSION

In this section we apply the numerical method presented above to obtain results for the electric susceptibility of helium atom as a function of time during the interaction with a short intense laser pulse. In all of our calculations we have used a Gaussian envelope for a 10 cycle full width at half maximum (FWHM) pulse at a central wavelength of 800 nm. The peak intensity of the pulse is varied from 1.5×10^{14} W/cm^2 to 3×10^{14} W/cm^2. In Fig. 1 we present the results for four different intensities (in TW/cm^2): 300 (solid line), 250 (dashed line), 200 (dotted line), and 150 (dashed-dotted line) as a function of time, which is scaled in terms of the cycle of the electric field. Results are shown for the middle 16 cycles of

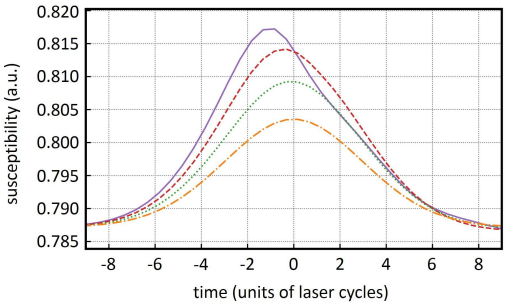

FIG. 1: (Color online) Time dependent susceptibility of helium interacting with intense laser pulses at a wavelength of 800 nm and a pulse length of 10 cycles (FWHM of Gaussian envelope). Peak intensities are 150 TW/cm^2 (dashed-dotted line), 200 TW/cm^2 (dotted line), 250 TW/cm^2 (dashed line) and 300 TW/cm^2 (solid line). Time is given in terms of the electric field cycle, where $t = 0$ cycles denotes the center of the pulse.

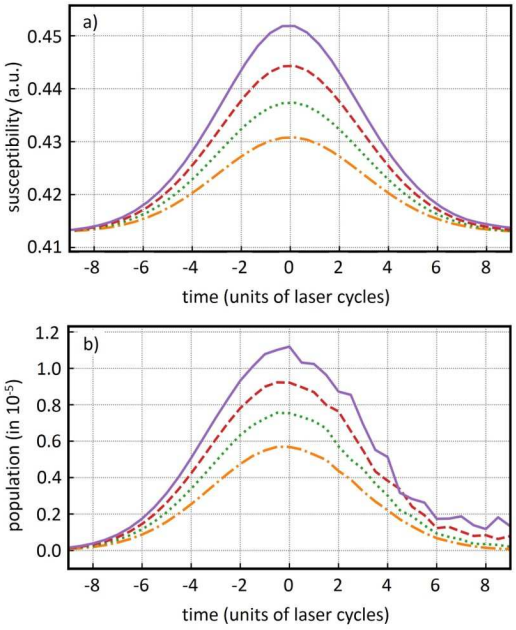

FIG. 2: (Color online) a) Field-free bound-bound contribution to the time dependent susceptibility and b) population in the field-free bound excited states of the spectrum, taken at the zeros of the driving field. Laser parameters and line styles are the same as in Fig. 1.

the field, where we have set $t = 0$ cycles to coincide with the peak of the electric field. Experimental data for the nonlinear refractive index have been obtained at similar intensities [20].

For the lower intensities ($150 - 200$ TW/cm^2), our results show that the susceptibility adiabatically follows the envelope of the field amplitude, i.e. properly scaled these results do coincide with the results of the (windowed) Gaussian envelope function. This is in agreement with the expectation from a perturbative electron-field interaction. Above 200 TW/cm^2, however, the results start to deviate from this adiabatic behavior. At 250 TW/cm^2 the peak of the susceptibility has slightly shifted away from the center of the field towards the beginning of the pulse, and at 300 TW/cm^2 it has moved by more than a full cycle of the driving field. This behavior is in qualitative agreement with results shown in the supplemental material of Ref. [20].

At the highest intensities considered, one can observe further deviations from the adiabatic behavior during the trailing part of the pulse. In both cases there is an additional change of concavity in the slope near $t = +1$ cycle, which initially appears at 250 TW/cm^2 and becomes more obvious at 300 TW/cm^2. At the latter intensity we also notice a second change at about $t = +5$ cycles. We note that the deviations from the adiabatic behavior occur at intensities at which previously a change in the nonlinear refractive index (e.g., [17, 30]) and a transition from perturbative to nonperturbative electron-field interaction [14] have been observed.

A. Analysis of time-dependent susceptibility

In order to obtain further insights into the results for the time-dependent susceptibility we first present in Fig. 2(a) the contributions related to the field-free bound parts of the spectrum. The results show that this contribution to the electric susceptibility follows almost adiabatically the envelope of the field. There is a small deviation at the highest intensities, at which the value at the end of the pulse is slightly larger than at the beginning of the pulse. This can be readily understood from the results for the population in the excited states, defined as all bound states except the ground state, which is presented in Fig. 2(b). This population (taken at the zeroes of the electric field) increases, adiabatically following the field envelope, in the rising part of the pulse, but one can see that the population does not completely return to zero in the trailing part of the pulse, leaving a residual excited state population at the end of the pulse. The amount of the residual population, as one would expect, increases with an increase of the intensity of the pulse and explains the differences between the bound-bound contribution to the total susceptibility at the beginning and at the end of the pulse.

The contribution to the time-dependent susceptibility, shown in Fig. 2, is the largest term and therefore accounts for the overall shape of the total susceptibility. Indeed, at the lowest intensities, it almost entirely gives rise to the adiabatic form, which closely follows the envelope of the electric field. For the deviations from field-following behavior, specifically the features we pointed out earlier at higher intensities (c.f., Fig. 1), we will now turn to the other contributions in Eq. (11).

The contribution to the time dependent susceptibility from the continuum part of the field-free spectrum is

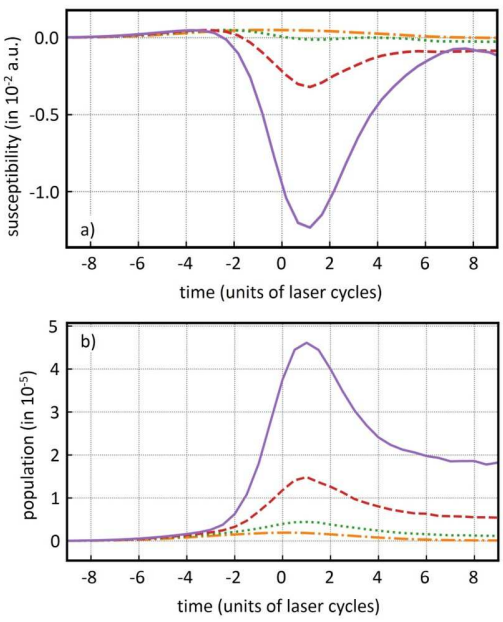

FIG. 3: (Color online) Same as Fig. 2, but for the continuum part of the field-free spectrum.

shown in Fig. 3(a), accompanied by the population in the field-free continuum states taken at the zeros of the driving electric field (Fig. 3(b)). At the lowest intensity (150 TW/cm^2, dashed-dotted curve), the shape of the susceptibility as a function of time is adiabatic, and positive, though small. At these intensities, the population in the field-free continuum states is mainly transient during the pulse and there is almost no residual population in the continuum at the end of the pulse.

In contrast, at the highest intensities, 250 TW/cm^2 (dashed line) and 300 TW/cm^2 (solid line), we observe a much stronger population of the field-free continuum states which continues to increase beyond the peak of the pulse up to $t = +1$ cycle. As one would expect, the onset for the continuum population appears earlier in the pulse and the continuum population is larger as the intensity of the laser pulse increases. The fast rise of the continuum population over a short interaction time is also a signature for a change to a nonperturbative field interaction. In agreement with previous results [14] we observe this behavior for the interaction of a helium atom with a laser field at 800 nm in an intensity regime of $2-3\times10^{14}$ W/cm^2. In the remaining part of the trailing edge of the pulse there is a decrease until about $t = +5$ cycle, and the remaining population in the continuum at the end of the pulse corresponds to ionization. We note that this transfer back from the continuum to the bound (excited) states of the atom in the trailing part of the pulse has been observed before (e.g., [26, 31, 32]).

The trends in the continuum population are reflected in the corresponding contribution to the electric susceptibility (Fig. 3(a)) at the highest intensities. For example, there is a minimum, corresponding to the negative contribution from the continuum part to the susceptibility, at about $t = +1$ cycle. Furthermore, the features in the contribution from the field-free continuum states at the highest intensities can well explain the signatures we pointed out in the total susceptibility (Fig. 1). The strong growth in the continuum population (and corresponding negative contribution from the continuum contributions to the susceptibility) shows up in the total susceptibility as a shift in the peak of the susceptibility towards earlier times in the pulse, which confirms the explanation given by Wahlstrand et al. [20]. The peak in the population (and the corresponding minimum in the susceptibility) at around +1 cycle relates to the first change in concavity observed in the electric susceptibility during the trailing part of the pulse. On the other hand, the second change at about $t = +5$ cycles at 300 TW/cm^2 (Fig. 1) corresponds to the slow down in the back transfer of population from the continuum to the bound excited states.

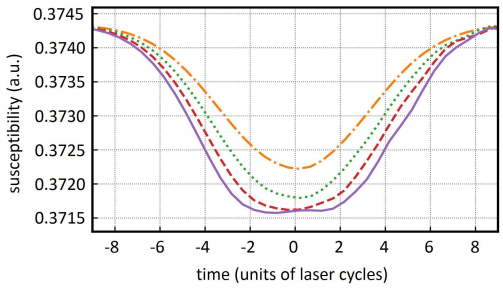

FIG. 4: (Color online) Same as Fig. 2a) but for the cross-term contributions.

Finally, the contributions to the susceptibility from the cross terms (between field-free bound and continuum states, c.f. Eq. (11)) are shown in Fig. 4. We observe a field envelope following negative contribution and small deviations at higher intensities. Overall, the variation in this contribution is however small and, hence, it is not important for the understanding of the dynamic features seen in the total susceptibility.

B. Role of orbital angular momentum

As mentioned previously, we attribute the nonadiabatic signatures in the total susceptibility at high intensities as due to a transition from perturbative to nonperturbative interaction of the field with the target atom. In particular, the population of the continuum states clearly shows features of a nonperturbative interaction, e.g. the exponential growth in continuum state population over a short interaction time. Although it is difficult to further separate perturbative and nonperturbative effects in our ab-initio calculations, we noticed that the transition between the corresponding regimes is related to a population of states with angular momentum quantum number

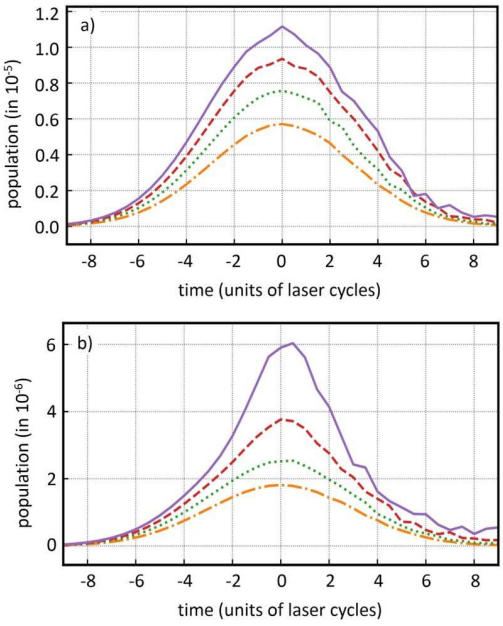

FIG. 5: (Color online) Population in (a) field-free bound states and (b) field-free continuum states with $l \leq 1$. The lines represent the results of calculations for pulses with peak intensity 150 TW/cm^2 (dashed-dotted line), 200 TW/cm^2 (dotted line), 250 TW/cm^2 (dashed line), and 300 TW/cm^2 (solid line).

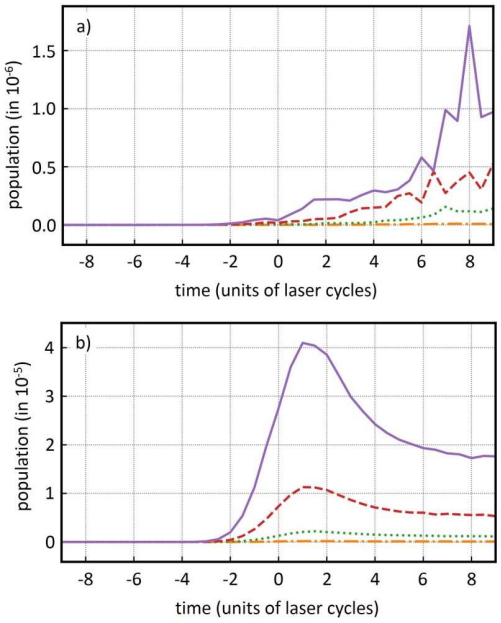

FIG. 6: (Color online) Same as Fig. 5, but for $l > 1$.

larger than 1.

To show this characteristic feature we present in Figs. 5 and 6 the populations in the field-free excited bound states (panels (a)) and continuum states (panels(b)), recorded at the zeroes of the field, for all states with $l \leq 1$ (Fig. 5) and for all states with $l > 1$ (Fig. 6). At all intensities considered the population in the low angular momentum states adiabatically follows the field envelope, while the population in the higher l-states mainly occurs in the trailing part of the pulse. Moreover, the latter population is predominantly observed at higher intensities. The results in Fig. 6(a) also show that the trapping in excited states during the trailing part of the pulse, seen in various previous studies (e.g., [26, 31, 32]), appears to have significant contributions from states with $l \geq 2$.

The same characteristic difference can be seen in the contributions to the total electric susceptibility, shown in Fig. 7. While the contributions from states with low angular momentum follow adiabatically the field envelope (panel a), in agreement with expectations from lowest-order perturbation theory, those from states with high angular momenta (panel b) clearly deviate from this behavior, in particular at the highest intensities considered. All the characteristic features that we pointed out at the outset of this section can thereofore be related to the slope of the high l-state contributions.

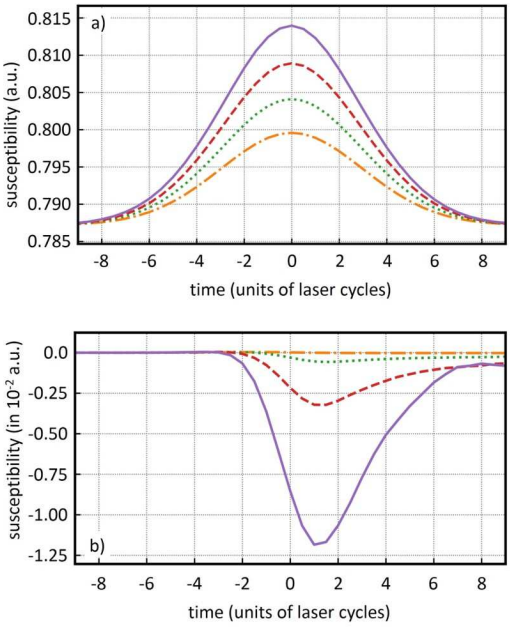

FIG. 7: (Color online) Contributions to the total susceptibility from (a) low ($l \leq 1$) and (b) high ($l > 1$) angular momentum states. Laser parameters and line styles as in Fig. 5.

IV. SUMMARY

We have presented a theoretical analysis of the time-dependent electric susceptibility of helium atom interacting with a short intense laser pulse. The analysis is based on numerical results using an expansion of the time-dependent wavefunction in a set of basis states and

the application of the short-time Fourier transform. In agreement with recent experimental data, the theoretical predictions show deviations from the adiabatic (field-following) behavior, expected from lowest-order perturbation theory, at the highest intensities considered. The shift in the peak towards the front of the pulse and the changes in the concavity of the slope in the trailing edge of the pulse have been related to the population in the field-free continuum states and bound excited states with high angular momentum due to a non-perturbative interaction between the atom and the electric field of the laser pulse. The conclusions do not depend on the characteristics of the ground state of the target and are expected to hold for other rare gas atoms as well.

Acknowledgments

This work was supported by MURI grants from the Air Force Office for Scientific Research (Award Nos. FA9550-10-1-0561 and FA 9550-16-1-0121) and by the JILA Physics Frontier Center grant from the U.S. National Science Foundation (Award No. PHY-1125844). We utilized the Janus supercomputer, which is supported by the National Science Foundation (Award No. CNS-0821794) and the University of Colorado Boulder. The Janus Supercomputer is a joint effort of the University of Colorado Boulder, the University of Colorado Denver, and the National Center for Atmospheric Research. Janus is operated by the University of Colorado Boulder.

[1] R.W. Boyd, *Nonlinear Optics*, 3rd ed. (Academic Press, Oxford, 2008).
[2] T. Brabec and F. Krausz, Rev. Mod. Phys. **72**, 545 (2000).
[3] T. Popmintchev, M.-C. Chen, P. Arpin, M.M. Murnane, H.C. Kapteyn, Nat. Photon. **4**, 822 (2010).
[4] D. Popmintchev, C. Hernandez-Garca, F. Dollar, C. Mancuso, J. Perez-Hernandez, M.C. Chen, A. Hankla, X. Gao, B. Shim, A. Gaeta, M. Tarazkar, D. Romanov, R. Levis, J. Gaffney, M. Foord, S. Libby, A. Jaron-Becker, A. Becker, L. Plaja, M. Murnane, H. Kapteyn, and T. Popmintchev, Science **350**, 1225 (2015).
[5] A. Couairon and A. Mysyrowicz, Phys. Rep. **441**, 47 (2007).
[6] L. Berge, S. Skupin, P. Nuter, J. Kasparian, and J.-P. Wolf, Rep. Prog. Phys. **70**, 1633 (2007).
[7] M. Kolesik and J.V. Moloney, Rep. Prog. Phys. **77**, 016401 (2014).
[8] P. Bejot, J. Kasparian, S. Henin, V. Loriot, T. Vieillard, E. Hertz, O. Faucher, B. Lavorel, and J. P. Wolf, Phys. Rev. Lett. **104**, 103903 (2010).
[9] M. Kolesik, E. M. Wright, and J. V. Moloney, Opt. Lett. **35**, 2550 (2010).
[10] P. Polynkin, M. Kolesik, E. M. Wright, and J. V. Moloney, Phys. Rev. Lett. **106**, 153902 (2011).
[11] P. Bejot, E. Hertz, J. Kasparian, B. Lavorel, J.-P. Wolf, and O. Faucher, Phys. Rev. Lett. **106**, 243902 (2011).
[12] C. Bree, A. Demircan, and G. Steinmeyer, Phys. Rev. Lett. **106**, 183902 (2011).
[13] C.K. Köhler, R. Guichard, E. Lorin, S. Chelkowski, A.D. Bandrauk, L. Berge, and S. Skupin, Phys. Rev. A **87**, 043811 (2013).
[14] A. Spott, A. Jaron-Becker, and A. Becker, Phys. Rev. A **90**, 013426 (2014).
[15] M. Tarazkar, D.A. Romanov, and R.J. Levis Phys. Rev. A **90**, 062514 (2014).
[16] A. Spott, A. Becker, and A. Jaron-Becker, Phys. Rev. A **91**, 023402 (2015).
[17] V. Loriot, E. Hertz, O. Faucher, and B. Lavorel, Opt. Express **17**, 13429 (2009); Opt. Express **18**, 3011 (2010).
[18] J.K. Wahlstrand, Y.-H. Cheng, Y.-H. Chen, and H.M. Milchberg, Phys. Rev. Lett. **107**, 103911 (2011).
[19] J.K. Wahlstrand, Y.-H. Cheng, and H.M. Milchberg, Phys. Rev. A **85**, 043820 (2012).
[20] J.K. Wahlstrand, Y.-H. Cheng, and H.M. Milchberg, Phys. Rev. Lett. **109**, 113904 (2012).
[21] P. Agostini, F.Fabre, G. Mainfray, G. Petite, and N.K. Rahman, Phys. Rev. Lett. **42**, 1127 (1979).
[22] G. Petite, P. Agostini, and H.G. Muller, J. Phys. B: At. Mol. Opt. Phys. **21**, 4097 (1988).
[23] A. McPherson, G. Gibson, H. Jara, T.S. Luk, I.A. McIntyre, K. Boyer, and C.K. Rhodes, J. Opt. Soc. Am. B **4**, 595 (1987).
[24] M. Ferray, A. L'Huillier, X.F. Li, L.A. Lompre, G. Mainfray, and C. Manus, J. Phys. B **21**, L31 (1988).
[25] J. H. Odhner, D. A. Romanov, E. T. McCole, J. K. Wahlstrand, H. M. Milchberg, and R. J. Levis, Phys. Rev. Lett. **109**, 065003 (2012).
[26] S.H. Chen, X. Guo, Y. Li, A. Becker, and A. Jaroń-Becker, Phys. Rev. A **86**, 013410 (2012).
[27] C.L. Dolph, Proc. IRE **34**, 335 (1946).
[28] J.O. Smith III, *Spectral Audio Signal Processing* (Center for Computer Research in Music and Acoustics, Stanford University), https://ccrma.stanford.edu/ jos/sasp/
[29] X.M. Tong and C.D. Lin, J. Phys. B: At. Mol. Opt. Phys. **38**, 2593 (2005)
[30] M. Nurhuda, A. Suda, M. Hatayama, K. Nagasaka, and K. Midorikawa, Phys. Rev. A **66**, 023811 (2002).
[31] R.R. Jones, D.W. Schumacher, and P.H. Bucksbaum, Phys. Rev. A **47**, R49 (1993).
[32] T. Nubbemeyer, K. Gorling, A. Saenz, U. Eichmann, and W. Sandner, Phys. Rev. Lett. **101**, 233001 (2008).